Journal of Sound and Vibration (2002) **257**(2), 361–379
doi:10.1006/jsvi.5044, available online at http://www.idealibrary.com on IDEAL®

SUBSTRUCTURE SYNTHESIS VIA ELASTIC MEDIA

W. Liu and D. J. Ewins

Department of Mechanical Engineering, Imperial College of Science, Technology and Medicine, Exhibition Road, London SW7 2BX, England. E-mails: w.j.liu@ic.ac.uk; d.ewins@ic.ac.uk

(*Received* 3 *May* 2001, *and in final form* 5 *December* 2001)

This paper presents a brief review of previous developments in substructure synthesis methods using frequency response functions and proposes a new coupling analysis approach which takes into account the effect of elastic media between substructures—the so-called general joint description method (GJDM). The theoretical basis of the new method is presented here and applications are demonstrated via two numerical simulations. The elastic media between substructures, i.e., the joints, are described by general impedance matrices which have only boundary degrees of freedom. The introduction of elastic media into coupling analyses can reduce errors caused by improper treatment of joints in conventional coupling analysis methods and can also provide a solution for non-conforming interfaces, where the numbers of degrees of freedom at the interfaces of two substructures are not consistent. In addition, the new method enables the dynamic behaviour of an assembled structure be easily tuned by changing the joint parameters only. These advantages show that the GJDM is an efficient and versatile tool in substructure synthesis analyses.

1. INTRODUCTION

Component mode synthesis (CMS) techniques have been developed and used extensively in the dynamic analysis of structures for over three decades. The original idea was to describe a structural system as an assembly of discrete structural components or substructures, thereby obtaining sets of matrix equations which predict the modal properties of the assembly. With the development of the finite element method and more powerful computers, the fundamental idea was then implemented and applied in practice in the 1960s and 1970s [1]. If CMS is mainly based on modal models derived either from spatial models, or resulting from a modal identification routine [2], the frequency response function (FRF)-based coupling method is then basically built on experimental models or, in other words, response models. In fact, since the different types of models can be interrelated with each other [3], both coupling methods allow the use of a combination of analytical and experimental data. Compared with the CMS method, FRF coupling has the advantage of being able to use the measured FRFs directly, which implies that all errors introduced by modal analysis, and the errors caused by high mode truncation, could be eliminated since the effects of the higher modes are naturally included in the measured response data.

The widely used expression of the FRF coupling method [4] connects two substructures rigidly at the coupling co-ordinates. Other coupling methods, either in the group of impedance coupling (spatial coupling method) or modal coupling (free interface and fixed interface methods), follow the same compatibility condition of displacement as well.

0022-460X/02/$35.00

To refine the general coupling analysis techniques, more researches on some specific aspects have been carried out. For instance, Otte *et al.* [5] proposed two data reduction methods to enhance measured FRFs for coupling in the spatial and frequency domains, respectively, since the computed FRFs of an assembled structure may be contaminated by errors. These methods are based on singular-value decomposition (SVD) and resolve the problems of ill-conditioned matrix inversion and the influence of noise. Three sources of error are normally encountered: (1) the inconsistencies of measured data (noise, frequency shifts), (2) the inability to measure correctly all d.o.f.s of the connection, and (3) the ill-conditioned matrix inversion for a large numbers of d.o.f.s. Suatez [6] introduced a force derivative method to compensate for the effect of the truncated higher modes in the representation of the substructures' response. It was demonstrated that the method is capable of providing very accurate estimates of the natural frequencies of the combined structure as well as the associated modes of vibration and elastic forces.

It is worth pointing out here that the essential principles in those methods mentioned above are similar to the FRF coupling method in respect of their treatment of the connections between substructures, i.e., they presume the same compatibility conditions of displacement at the interfaces of the connections. The substructures for numerical simulation were designed to meet the required conditions and, therefore, the solutions of coupled structure analysis were satisfactory. Practically, however, the accurate analysis of coupled structures requires not only high-quality substructure data estimation but also the reliable modelling of the joints which connect the substructures. If the rigid connection assumption does not adequately describe the characteristics of realistic joints, it is clear that the FRFs obtained from the coupling analysis will certainly differ from the experimental results of the corresponding assembled structure, no matter how fine the algorithms are.

Basically, the theory of coupled structure analysis developed so far has not taken full account of the effect of practical joints. The effect of joints should be estimated carefully and the joint models should be established and the theory of substructure coupling analysis should be developed further to include proper joint effects.

2. REVIEW OF THE ESSENTIAL PRINCIPLES

The currently used FRF coupling method was systematically presented by Jetmundsen *et al.* [4] but the initial idea of the method can be traced back to 1960 in the book by Bishop and Johnson [7].

2.1. FRF COUPLING WITHOUT JOINT

The conventional mathematical expression of FRF coupling method is well known [4] as

$$\mathbf{H} = \begin{bmatrix} {}_A\mathbf{H}_{ii} & {}_A\mathbf{H}_{ic} & \mathbf{0} \\ {}_A\mathbf{H}_{ci} & {}_A\mathbf{H}_{cc} & \mathbf{0} \\ \mathbf{0} & \mathbf{0} & {}_B\mathbf{H}_{ii} \end{bmatrix} - \begin{bmatrix} {}_A\mathbf{H}_{ic} \\ {}_A\mathbf{H}_{cc} \\ -{}_B\mathbf{H}_{ic} \end{bmatrix} [{}_A\mathbf{H}_{cc} + {}_B\mathbf{H}_{cc}]^{-1} [{}_A\mathbf{H}_{ci} \quad {}_A\mathbf{H}_{cc} \quad -{}_B\mathbf{H}_{ci}], \quad (1)$$

in which $\mathbf{H}$ is the FRF matrix of the assembled structure, ${}_A\mathbf{H}$, ${}_B\mathbf{H}$ are the FRF matrices of substructures A and B, respectively. Subscript i represents internal d.o.f.s and c denotes the coupling (interface) d.o.f.s.

If the FRF matrix of the coupled structure has the form

$$\mathbf{H} = \begin{bmatrix} \mathbf{H}_{aa} & \mathbf{H}_{ac} & \mathbf{H}_{ab} \\ \mathbf{H}_{ca} & \mathbf{H}_{cc} & \mathbf{H}_{cb} \\ \mathbf{H}_{ba} & \mathbf{H}_{bc} & \mathbf{H}_{bb} \end{bmatrix}, \tag{2}$$

then each submatrix can be expressed individually as

$$\begin{aligned}
\mathbf{H}_{aa} &= {}_A\mathbf{H}_{ii} - {}_A\mathbf{H}_{ic}[{}_A\mathbf{H}_{cc} + {}_B\mathbf{H}_{cc}]^{-1}\,{}_A\mathbf{H}_{ci}, \\
\mathbf{H}_{ac} &= {}_A\mathbf{H}_{ic} - {}_A\mathbf{H}_{ic}[{}_A\mathbf{H}_{cc} + {}_B\mathbf{H}_{cc}]^{-1}\,{}_A\mathbf{H}_{cc}, \\
\mathbf{H}_{ab} &= {}_A\mathbf{H}_{ic}[{}_A\mathbf{H}_{cc} + {}_B\mathbf{H}_{cc}]^{-1}\,{}_B\mathbf{H}_{ci}, \\
\mathbf{H}_{cc} &= {}_A\mathbf{H}_{cc} - {}_A\mathbf{H}_{cc}[{}_A\mathbf{H}_{cc} + {}_B\mathbf{H}_{cc}]^{-1}\,{}_A\mathbf{H}_{cc}, \\
\mathbf{H}_{cb} &= {}_A\mathbf{H}_{cc}[{}_A\mathbf{H}_{cc} + {}_B\mathbf{H}_{cc}]^{-1}\,{}_B\mathbf{H}_{ci}, \\
\mathbf{H}_{bb} &= {}_B\mathbf{H}_{ii} - {}_B\mathbf{H}_{ic}[{}_A\mathbf{H}_{cc} + {}_B\mathbf{H}_{cc}]^{-1}\,{}_B\mathbf{H}_{ci}
\end{aligned} \tag{3}$$

and by symmetry,

$$\mathbf{H}_{ca} = \mathbf{H}_{ac}^{\mathrm{T}}, \qquad \mathbf{H}_{ba} = \mathbf{H}_{ab}^{\mathrm{T}}, \qquad \mathbf{H}_{bc} = \mathbf{H}_{cb}^{\mathrm{T}}. \tag{4}$$

2.2. FRF COUPLING WITH JOINT

The FRF coupling method presented in equation (1) does not allow for the effect of any medium between substructures. A method of FRF coupling with joints was recently reported by Ferreira [8], in which the description of substructures and their assembly is the same as that mentioned in reference [9]. The new development of the method in reference [8], in respect of the substructure coupling analysis, lies in the joint description and synthesis with substructures. However, it can be seen in the derivation process of the coupling method in reference [8] that the expressions for the forces applied on the substructures, $\mathbf{f}_{\bar{c}}$ and $\mathbf{f}_{\tilde{c}}$, are not unique. It seems that the solution should be consistent only if the joint describing function, $\mathbf{Z}$, is infinite or, in other words, if $\mathbf{Z}^{-1} = 0$. Obviously, this condition conflicts with the purpose of the coupling analysis and, therefore, there must be an error in the derivation.

In fact, the joint model expression given in reference [8] is

$$-\begin{Bmatrix} \mathbf{f}_{\bar{c}} \\ \mathbf{f}_{\tilde{c}} \end{Bmatrix} = \begin{bmatrix} \mathbf{Z} & -\mathbf{Z} \\ -\mathbf{Z} & \mathbf{Z} \end{bmatrix} \begin{Bmatrix} \mathbf{x}_{\bar{c}} \\ \mathbf{x}_{\tilde{c}} \end{Bmatrix}. \tag{5}$$

This joint model is based on two essential assumptions (which are not explicitly mentioned in reference [8]): the first assumption is that the equilibrium and compatibility conditions are given in the form of

$$\begin{Bmatrix} \mathbf{f}_{\bar{c}} \\ \mathbf{f}_{\tilde{c}} \end{Bmatrix} = -\begin{Bmatrix} \bar{\boldsymbol{f}} \\ \tilde{\boldsymbol{f}} \end{Bmatrix} \quad \text{and} \quad \begin{Bmatrix} \mathbf{x}_{\bar{c}} \\ \mathbf{x}_{\tilde{c}} \end{Bmatrix} = \begin{Bmatrix} \bar{\boldsymbol{x}} \\ \tilde{\boldsymbol{x}} \end{Bmatrix} \tag{6}$$

and the second assumption is that the stiffness matrix of the joint has to take the specific form of

$$\boldsymbol{K} = \begin{bmatrix} \mathbf{Z} & -\mathbf{Z} \\ -\mathbf{Z} & \mathbf{Z} \end{bmatrix}. \tag{7}$$

Expression (5) implies that the joints between the substructures can only be parallel scalar massless springs and/or dampers.

According to the proposed equilibrium conditions in reference [8], the external forces applied at the interfaces of the assembled structure have always to be zero:

$$\mathbf{F}_{\bar{C}} = \mathbf{F}_{\tilde{C}} = \mathbf{f}_{\bar{c}} + \mathbf{f}_{\tilde{c}} \equiv \mathbf{0}. \tag{8}$$

Therefore, when these basic assumptions are used in the derivations, the two sets of forces, $\mathbf{F}_{\bar{c}}$ and $\mathbf{F}_{\tilde{c}}$, appearing in the expressions of $\mathbf{f}_{\bar{c}}$ and $\mathbf{f}_{\tilde{c}}$, can have arbitrary coefficients without affecting the values of $\mathbf{f}_{\bar{c}}$ and $\mathbf{f}_{\tilde{c}}$. That is why the solutions are not unique.

3. GENERAL JOINT DESCRIPTION METHOD—NEW DEVELOPMENT

3.1. BACKGROUND THEORY

To correct the equilibrium condition used in reference [8], and to employ a general joint description matrix, a generalized joint description method (GJDM) for substructure coupling analysis is derived in this section, starting from joint description.

3.1.1. *Joint description*

A joint can be analytically described as

$$\boldsymbol{f} = \boldsymbol{Z}\boldsymbol{x}, \tag{9}$$

where

$$\boldsymbol{f} = \begin{Bmatrix} \bar{\boldsymbol{f}} \\ \tilde{\boldsymbol{f}} \end{Bmatrix}, \qquad \boldsymbol{x} = \begin{Bmatrix} \boldsymbol{x}_{\bar{c}} \\ \boldsymbol{x}_{\tilde{c}} \end{Bmatrix} \tag{10}$$

and $\boldsymbol{Z}$ is the impedance matrix of the joint. Since it is normally symmetric, such that

$$\boldsymbol{Z} = \begin{bmatrix} \boldsymbol{Z}_{\bar{c}\bar{c}} & \boldsymbol{Z}_{\bar{c}\tilde{c}} \\ \boldsymbol{Z}_{\tilde{c}\bar{c}} & \boldsymbol{Z}_{\tilde{c}\tilde{c}} \end{bmatrix} \tag{11}$$

with $\boldsymbol{Z}_{\bar{c}\bar{c}} = \boldsymbol{Z}_{\bar{c}\bar{c}}^{\mathrm{T}}$, $\boldsymbol{Z}_{\bar{c}\tilde{c}} = \boldsymbol{Z}_{\tilde{c}\bar{c}}^{\mathrm{T}}$ and $\boldsymbol{Z}_{\tilde{c}\tilde{c}} = \boldsymbol{Z}_{\tilde{c}\tilde{c}}^{\mathrm{T}}$.

The joint has no internal degrees of freedom: all of its degrees of freedom are on its boundaries. If the number of degrees of freedom at the boundary of substructure A equals that on the boundary of substructure B, then $n_{\bar{c}} = n_{\tilde{c}}$, and $\boldsymbol{Z}_{\bar{c}\tilde{c}}$ is a square matrix. Otherwise, in more general cases, if $n_{\bar{c}} \neq n_{\tilde{c}}$, $\boldsymbol{Z}_{\bar{c}\tilde{c}}$ is rectangular.

3.1.2. *Conditions of compatibility and equilibrium*

The displacement vector of the joint, $\boldsymbol{x}$, satisfies the compatibility condition

$$\begin{Bmatrix} \boldsymbol{x}_{\bar{c}} \\ \boldsymbol{x}_{\tilde{c}} \end{Bmatrix} = \begin{Bmatrix} \mathbf{x}_{\bar{c}} \\ \mathbf{x}_{\tilde{c}} \end{Bmatrix} \tag{12}$$

and the force vector, $\boldsymbol{f}$, satisfies the equilibrium condition at the coupling interfaces

$$\begin{Bmatrix} \mathbf{f}_{\bar{c}} \\ \mathbf{f}_{\tilde{c}} \end{Bmatrix} = \begin{Bmatrix} \mathbf{F}_{\bar{C}} \\ \mathbf{F}_{\tilde{C}} \end{Bmatrix} - \begin{Bmatrix} \bar{\boldsymbol{f}} \\ \tilde{\boldsymbol{f}} \end{Bmatrix}, \tag{13}$$

where $\mathbf{F}_{\bar{C}}$ and $\mathbf{F}_{\tilde{C}}$ are the external forces acting on the interface d.o.f.s. When there are no external forces applied on the interface d.o.f.s, equation (13) becomes

$$\boldsymbol{f} = -\begin{Bmatrix} \mathbf{f}_{\bar{c}} \\ \\ \mathbf{f}_{\tilde{c}} \end{Bmatrix}. \tag{14}$$

3.1.3. *Description of substructures*

To describe each of the uncoupled substructures, one can write the displacement vector as

$$\begin{Bmatrix} \mathbf{x}_i \\ \mathbf{x}_{\bar{c}} \\ \mathbf{x}_{\tilde{c}} \end{Bmatrix} = \begin{bmatrix} \mathbf{H}_{ii} & \mathbf{H}_{i\bar{c}} & \mathbf{H}_{i\tilde{c}} \\ \mathbf{H}_{\bar{c}i} & \mathbf{H}_{\bar{c}\bar{c}} & \mathbf{H}_{\bar{c}\tilde{c}} \\ \mathbf{H}_{\tilde{c}i} & \mathbf{H}_{\tilde{c}\bar{c}} & \mathbf{H}_{\tilde{c}\tilde{c}} \end{bmatrix} \begin{Bmatrix} \mathbf{f}_i \\ \mathbf{f}_{\bar{c}} \\ \mathbf{f}_{\tilde{c}} \end{Bmatrix}. \tag{15}$$

3.1.4. *Derivation of the receptance matrix of the coupled structure*

Solving for $\mathbf{x}_{\bar{c}}$ and $\mathbf{x}_{\tilde{c}}$ from equation (15) and substituting these into equation (9), gives

$$\boldsymbol{Z}_{\bar{c}\bar{c}}(\mathbf{H}_{\bar{c}i}\mathbf{f}_i + \mathbf{H}_{\bar{c}\bar{c}}\mathbf{f}_{\bar{c}} + \mathbf{H}_{\bar{c}\tilde{c}}\mathbf{f}_{\tilde{c}}) + \boldsymbol{Z}_{\bar{c}\tilde{c}}(\mathbf{H}_{\tilde{c}i}\mathbf{f}_i + \mathbf{H}_{\tilde{c}\bar{c}}\mathbf{f}_{\bar{c}} + \mathbf{H}_{\tilde{c}\tilde{c}}\mathbf{f}_{\tilde{c}}) = \bar{\boldsymbol{f}} = \mathbf{0}, \tag{16}$$

$$\boldsymbol{Z}_{\tilde{c}\bar{c}}(\mathbf{H}_{\bar{c}i}\mathbf{f}_i + \mathbf{H}_{\bar{c}\bar{c}}\mathbf{f}_{\bar{c}} + \mathbf{H}_{\bar{c}\tilde{c}}\mathbf{f}_{\tilde{c}}) + \boldsymbol{Z}_{\tilde{c}\tilde{c}}(\mathbf{H}_{\tilde{c}i}\mathbf{f}_i + \mathbf{H}_{\tilde{c}\bar{c}}\mathbf{f}_{\bar{c}} + \mathbf{H}_{\tilde{c}\tilde{c}}\mathbf{f}_{\tilde{c}}) - \tilde{\boldsymbol{f}} = \mathbf{0}. \tag{17}$$

Substituting equation (13) into equations (16) and (17), and noting that $\mathbf{f}_i = \mathbf{F}_I$, one has

$$\boldsymbol{Z}_{\bar{c}\bar{c}}(\mathbf{H}_{\bar{c}i}\mathbf{F}_I + \mathbf{H}_{\bar{c}\bar{c}}\mathbf{f}_{\bar{c}} + \mathbf{H}_{\bar{c}\tilde{c}}\mathbf{f}_{\tilde{c}}) + \boldsymbol{Z}_{\bar{c}\tilde{c}}(\mathbf{H}_{\tilde{c}i}\mathbf{F}_I + \mathbf{H}_{\tilde{c}\bar{c}}\mathbf{f}_{\bar{c}} + \mathbf{H}_{\tilde{c}\tilde{c}}\mathbf{f}_{\tilde{c}}) - \mathbf{F}_{\bar{C}} + \mathbf{f}_{\bar{c}} = \mathbf{0}, \tag{18}$$

$$\boldsymbol{Z}_{\tilde{c}\bar{c}}(\mathbf{H}_{\bar{c}i}\mathbf{F}_I + \mathbf{H}_{\bar{c}\bar{c}}\mathbf{f}_{\bar{c}} + \mathbf{H}_{\bar{c}\tilde{c}}\mathbf{f}_{\tilde{c}}) + \boldsymbol{Z}_{\tilde{c}\tilde{c}}(\mathbf{H}_{\tilde{c}i}\mathbf{F}_I + \mathbf{H}_{\tilde{c}\bar{c}}\mathbf{f}_{\bar{c}} + \mathbf{H}_{\tilde{c}\tilde{c}}\mathbf{f}_{\tilde{c}}) - \mathbf{F}_{\tilde{C}} + \mathbf{f}_{\tilde{c}} = \mathbf{0}. \tag{19}$$

Rearranging these two equations with respect to the force vectors, gives

$$\mathbf{a}_1\mathbf{f}_{\bar{c}} + \mathbf{a}_2\mathbf{f}_{\tilde{c}} = \mathbf{F}_{\bar{C}} - \mathbf{a}_3\mathbf{F}_I, \qquad \mathbf{b}_1\mathbf{f}_{\bar{c}} + \mathbf{b}_2\mathbf{f}_{\tilde{c}} = \mathbf{F}_{\tilde{C}} - \mathbf{b}_3\mathbf{F}_I. \tag{20, 21}$$

Solving equations (20) and (21), one obtains the force vectors for the uncoupled system uniquely expressed in terms of the external force vectors of the coupled system as

$$\mathbf{f}_{\bar{c}} = \bar{\mathbf{B}}^{-1}[(\mathbf{b}_3 - \mathbf{b}_2\mathbf{a}_2^{-1}\mathbf{a}_3)\mathbf{F}_I + \mathbf{b}_2\mathbf{a}_2^{-1}\mathbf{F}_{\bar{C}} - \mathbf{F}_{\tilde{C}}], \tag{22}$$

$$\mathbf{f}_{\tilde{c}} = \tilde{\mathbf{B}}^{-1}[(\mathbf{a}_3 - \mathbf{a}_1\mathbf{b}_1^{-1}\mathbf{b}_3)\mathbf{F}_I - \mathbf{F}_{\bar{C}} + \mathbf{a}_1\mathbf{b}_1^{-1}\mathbf{F}_{\tilde{C}}], \tag{23}$$

where

$$\mathbf{a}_1 = \boldsymbol{Z}_{\bar{c}\bar{c}}\mathbf{H}_{\bar{c}\bar{c}} + \boldsymbol{Z}_{\bar{c}\tilde{c}}\mathbf{H}_{\tilde{c}\bar{c}} + \mathbf{I}, \quad \mathbf{a}_2 = \boldsymbol{Z}_{\bar{c}\bar{c}}\mathbf{H}_{\bar{c}\tilde{c}} + \boldsymbol{Z}_{\bar{c}\tilde{c}}\mathbf{H}_{\tilde{c}\tilde{c}}, \quad \mathbf{a}_3 = \boldsymbol{Z}_{\bar{c}\bar{c}}\mathbf{H}_{\bar{c}i} + \boldsymbol{Z}_{\bar{c}\tilde{c}}\mathbf{H}_{\tilde{c}i},$$

$$\mathbf{b}_1 = \boldsymbol{Z}_{\tilde{c}\bar{c}}\mathbf{H}_{\bar{c}\bar{c}} + \boldsymbol{Z}_{\tilde{c}\tilde{c}}\mathbf{H}_{\tilde{c}\bar{c}}, \quad \mathbf{b}_2 = \boldsymbol{Z}_{\tilde{c}\bar{c}}\mathbf{H}_{\bar{c}\tilde{c}} + \boldsymbol{Z}_{\tilde{c}\tilde{c}}\mathbf{H}_{\tilde{c}\tilde{c}} + \mathbf{I}, \quad \mathbf{b}_3 = \boldsymbol{Z}_{\tilde{c}\bar{c}}\mathbf{H}_{\bar{c}i} + \boldsymbol{Z}_{\tilde{c}\tilde{c}}\mathbf{H}_{\tilde{c}i},$$

$$\bar{\mathbf{B}} = \mathbf{b}_2\mathbf{a}_2^{-1}\mathbf{a}_1 - \mathbf{b}_1, \quad \tilde{\mathbf{B}} = \mathbf{a}_1\mathbf{b}_1^{-1}\mathbf{b}_2 - \mathbf{a}_2. \tag{24}$$

Substituting equations (22) and (23) into equation (15), and using the following compatibility conditions:

$$\mathbf{X}_I = \mathbf{x}_i, \quad \mathbf{X}_{\bar{C}} = \mathbf{x}_{\bar{c}} \quad \text{and} \quad \mathbf{X}_{\tilde{C}} = \mathbf{x}_{\tilde{c}} \tag{25}$$

elements in the upper triangle part of the coupled structure's FRF matrix are obtained as follows:

$$\mathbf{H}_{II} = \mathbf{H}_{ii} + \mathbf{H}_{i\bar{c}}\bar{\mathbf{B}}^{-1}(\mathbf{b}_3 - \mathbf{b}_2\mathbf{a}_2^{-1}\mathbf{a}_3) + \mathbf{H}_{i\check{c}}\tilde{\mathbf{B}}^{-1}(\mathbf{a}_3 - \mathbf{a}_1\mathbf{b}_1^{-1}\mathbf{b}_3),$$

$$\mathbf{H}_{I\bar{C}} = \mathbf{H}_{i\bar{c}}\bar{\mathbf{B}}^{-1}\mathbf{b}_2\mathbf{a}_2^{-1} - \mathbf{H}_{i\check{c}}\tilde{\mathbf{B}}^{-1}, \quad \mathbf{H}_{I\check{C}} = \mathbf{H}_{i\check{c}}\tilde{\mathbf{B}}^{-1}\mathbf{a}_1\mathbf{b}_1^{-1} - \mathbf{H}_{i\bar{c}}\bar{\mathbf{B}}^{-1},$$

$$\mathbf{H}_{\bar{C}\bar{C}} = \mathbf{H}_{\bar{c}\bar{c}}\bar{\mathbf{B}}^{-1}\mathbf{b}_2\mathbf{a}_2^{-1} - \mathbf{H}_{\bar{c}\check{c}}\tilde{\mathbf{B}}^{-1}, \quad \mathbf{H}_{\bar{C}\check{C}} = \mathbf{H}_{\bar{c}\check{c}}\tilde{\mathbf{B}}^{-1}\mathbf{a}_1\mathbf{b}_1^{-1} - \mathbf{H}_{\bar{c}\bar{c}}\bar{\mathbf{B}}^{-1},$$

$$\mathbf{H}_{\check{C}\check{C}} = \mathbf{H}_{\check{c}\check{c}}\tilde{\mathbf{B}}^{-1}\mathbf{a}_1\mathbf{b}_1^{-1} - \mathbf{H}_{\check{c}\bar{c}}\bar{\mathbf{B}}^{-1}. \tag{26}$$

These FRF submatrices can be used to construct the receptance matrix of the coupled structure

$$\begin{Bmatrix} \mathbf{X}_I \\ \mathbf{X}_{\bar{C}} \\ \mathbf{X}_{\check{C}} \end{Bmatrix} = \begin{bmatrix} \mathbf{H}_{II} & \mathbf{H}_{I\bar{C}} & \mathbf{H}_{I\check{C}} \\ \mathbf{H}_{\bar{C}I} & \mathbf{H}_{\bar{C}\bar{C}} & \mathbf{H}_{\bar{C}\check{C}} \\ \mathbf{H}_{\check{C}I} & \mathbf{H}_{\check{C}\bar{C}} & \mathbf{H}_{\check{C}\check{C}} \end{bmatrix} \begin{Bmatrix} \mathbf{F}_I \\ \mathbf{F}_{\bar{C}} \\ \mathbf{F}_{\check{C}} \end{Bmatrix}, \tag{27}$$

where

$$\mathbf{H}_{\bar{C}I} = \mathbf{H}_{I\bar{C}}^{\mathrm{T}}, \qquad \mathbf{H}_{\check{C}I} = \mathbf{H}_{I\check{C}}^{\mathrm{T}}, \qquad \mathbf{H}_{\check{C}\bar{C}} = \mathbf{H}_{\bar{C}\check{C}}^{\mathrm{T}}. \tag{28}$$

3.2. ALGORITHM FOR IMPLEMENTATION OF THE THEORY

The expressions in (24) can be simplified by using the fact that

$$\mathbf{H}_{\bar{c}\check{c}} = \mathbf{H}_{\check{c}\bar{c}} = \mathbf{0}. \tag{29}$$

Substituting equation (29) into equation (24), we have

$$\mathbf{a}_1 = \boldsymbol{Z}_{\bar{c}\bar{c}}\mathbf{H}_{\bar{c}\bar{c}} + \mathbf{I}, \quad \mathbf{a}_2 = \boldsymbol{Z}_{\bar{c}\check{c}}\mathbf{H}_{\check{c}\check{c}}, \quad \mathbf{a}_3 = \boldsymbol{Z}_{\bar{c}\bar{c}}\mathbf{H}_{\bar{c}i} + \boldsymbol{Z}_{\bar{c}\check{c}}\mathbf{H}_{\check{c}i},$$

$$\mathbf{b}_1 = \boldsymbol{Z}_{\check{c}\bar{c}}\mathbf{H}_{\bar{c}\bar{c}}, \quad \mathbf{b}_2 = \boldsymbol{Z}_{\check{c}\check{c}}\mathbf{H}_{\check{c}\check{c}} + \mathbf{I}, \quad \mathbf{b}_3 = \boldsymbol{Z}_{\check{c}\bar{c}}\mathbf{H}_{\bar{c}i} + \boldsymbol{Z}_{\check{c}\check{c}}\mathbf{H}_{\check{c}i} \tag{30}$$

and

$$\bar{\mathbf{B}} = \mathbf{H}_{\bar{c}\check{c}}^{-1}\{\mathbf{H}_{\bar{c}\check{c}}(\boldsymbol{Z}_{\bar{c}\check{c}}\boldsymbol{Z}_{\bar{c}\check{c}}^{+}\boldsymbol{Z}_{\bar{c}\bar{c}} - \boldsymbol{Z}_{\bar{c}\check{c}})\mathbf{H}_{\bar{c}\bar{c}} + (\mathbf{H}_{\bar{c}\check{c}}\boldsymbol{Z}_{\check{c}\bar{c}}\boldsymbol{Z}_{\bar{c}\check{c}}^{+} + \boldsymbol{Z}_{\bar{c}\check{c}}^{+}\boldsymbol{Z}_{\bar{c}\check{c}}\mathbf{H}_{\bar{c}\bar{c}}) + \boldsymbol{Z}_{\bar{c}\check{c}}^{+}\},$$

$$\tilde{\mathbf{B}} = \mathbf{H}_{\bar{c}\check{c}}^{-1}\{\mathbf{H}_{\bar{c}\check{c}}(\boldsymbol{Z}_{\bar{c}\check{c}}\boldsymbol{Z}_{\bar{c}\check{c}}^{+}\boldsymbol{Z}_{\check{c}\check{c}} - \boldsymbol{Z}_{\bar{c}\check{c}})\mathbf{H}_{\check{c}\check{c}} + (\mathbf{H}_{\bar{c}\check{c}}\boldsymbol{Z}_{\check{c}\check{c}}\boldsymbol{Z}_{\bar{c}\check{c}}^{+} + \boldsymbol{Z}_{\bar{c}\check{c}}^{+}\boldsymbol{Z}_{\check{c}\check{c}}\mathbf{H}_{\check{c}\check{c}}) + \boldsymbol{Z}_{\bar{c}\check{c}}^{+}\}, \tag{31}$$

$$\bar{\mathbf{B}}^{+} = \{\mathbf{H}_{\check{c}\bar{c}}(\boldsymbol{Z}_{\check{c}\bar{c}}\boldsymbol{Z}_{\bar{c}\check{c}}^{+}\boldsymbol{Z}_{\bar{c}\bar{c}} - \boldsymbol{Z}_{\check{c}\bar{c}})\mathbf{H}_{\bar{c}\bar{c}} + (\mathbf{H}_{\check{c}\bar{c}}\boldsymbol{Z}_{\bar{c}\check{c}}\boldsymbol{Z}_{\bar{c}\check{c}}^{+} + \boldsymbol{Z}_{\bar{c}\check{c}}^{+}\boldsymbol{Z}_{\bar{c}\bar{c}}\mathbf{H}_{\bar{c}\bar{c}}) + \boldsymbol{Z}_{\bar{c}\check{c}}^{+}\}^{+}\mathbf{H}_{\check{c}\bar{c}},$$

$$\tilde{\mathbf{B}}^{+} = \{\mathbf{H}_{\bar{c}\check{c}}(\boldsymbol{Z}_{\bar{c}\check{c}}\boldsymbol{Z}_{\check{c}\check{c}}^{+}\boldsymbol{Z}_{\check{c}\check{c}} - \boldsymbol{Z}_{\bar{c}\check{c}})\mathbf{H}_{\check{c}\check{c}} + (\mathbf{H}_{\bar{c}\check{c}}\boldsymbol{Z}_{\check{c}\check{c}}\boldsymbol{Z}_{\check{c}\check{c}}^{+} + \boldsymbol{Z}_{\check{c}\check{c}}^{+}\boldsymbol{Z}_{\check{c}\check{c}}\mathbf{H}_{\check{c}\check{c}}) + \boldsymbol{Z}_{\check{c}\check{c}}^{+}\}^{+}\mathbf{H}_{\bar{c}\check{c}}. \tag{32}$$

Rewriting equation (32) in a short form, and comparing the expressions in the curly brackets, we note that if we denote

$$\bar{\mathbf{B}}^{+} = \mathbf{D}^{+}\mathbf{H}_{\check{c}\bar{c}}, \tag{33}$$

then

$$\tilde{\mathbf{B}}^{+} = (\mathbf{D}^{\mathrm{T}})^{+}\mathbf{H}_{\bar{c}\check{c}} = \mathbf{D}^{+\mathrm{T}}\mathbf{H}_{\bar{c}\check{c}}. \tag{34}$$

Therefore, the FRF submatrices of the coupled structure in equation (26) become

$$\mathbf{H}_{II} = \mathbf{H}_{ii} + \mathbf{H}_{i\tilde{c}}\mathbf{D}^{+}\mathbf{H}_{\tilde{c}\tilde{c}}(\mathbf{b}_3 - \mathbf{b}_2\mathbf{a}_2^{-1}\mathbf{a}_3) + \mathbf{H}_{i\bar{c}}\mathbf{D}^{+\mathrm{T}}\mathbf{H}_{\bar{c}\tilde{c}}(\mathbf{a}_3 - \mathbf{a}_1\mathbf{b}_1^{-1}\mathbf{b}_3),$$

$$\mathbf{H}_{I\bar{C}} = \mathbf{H}_{i\tilde{c}}\mathbf{D}^{+}\mathbf{H}_{\tilde{c}\bar{c}}\mathbf{b}_2\mathbf{a}_2^{-1} - \mathbf{H}_{i\bar{c}}\mathbf{D}^{+\mathrm{T}}\mathbf{H}_{\bar{c}\bar{c}},$$

$$\mathbf{H}_{I\tilde{C}} = \mathbf{H}_{i\bar{c}}\mathbf{D}^{+\mathrm{T}}\mathbf{H}_{\bar{c}\tilde{c}}\mathbf{a}_1\mathbf{b}_1^{-1} - \mathbf{H}_{i\tilde{c}}\mathbf{D}^{+}\mathbf{H}_{\tilde{c}\tilde{c}},$$

$$\mathbf{H}_{\bar{C}\bar{C}} = \mathbf{H}_{\bar{c}\tilde{c}}\mathbf{D}^{+}\mathbf{H}_{\tilde{c}\tilde{c}}\mathbf{b}_2\mathbf{a}_2^{-1},$$

$$\mathbf{H}_{\bar{C}\tilde{C}} = -\mathbf{H}_{\bar{c}\tilde{c}}\mathbf{D}^{+}\mathbf{H}_{\tilde{c}\tilde{c}}, \quad \mathbf{H}_{\tilde{C}\tilde{C}} = \mathbf{H}_{\tilde{c}\tilde{c}}\mathbf{D}^{+\mathrm{T}}\mathbf{H}_{\bar{c}\tilde{c}}\mathbf{a}_1\mathbf{b}_1^{-1}. \tag{35}$$

From equation (30), we have

$$\mathbf{b}_3 - \mathbf{b}_2\mathbf{a}_2^{-1}\mathbf{a}_3 = \mathbf{H}_{\tilde{c}\tilde{c}}^{-1}\{(\mathbf{H}_{\tilde{c}\tilde{c}}\mathbf{Z}_{\tilde{c}\bar{c}} - \mathbf{H}_{\tilde{c}\tilde{c}}\mathbf{Z}_{\tilde{c}\tilde{c}}\mathbf{Z}_{\tilde{c}\tilde{c}}^{+}\mathbf{Z}_{\tilde{c}\bar{c}} - \mathbf{Z}_{\tilde{c}\tilde{c}}^{+}\mathbf{Z}_{\tilde{c}\bar{c}})\mathbf{H}_{\bar{c}i} - \mathbf{H}_{\tilde{c}i}\},$$

$$\mathbf{a}_3 - \mathbf{a}_1\mathbf{b}_1^{-1}\mathbf{b}_3 = \mathbf{H}_{\bar{c}\tilde{c}}^{-1}\{(\mathbf{H}_{\bar{c}\tilde{c}}\mathbf{Z}_{\tilde{c}\tilde{c}} - \mathbf{H}_{\bar{c}\tilde{c}}\mathbf{Z}_{\tilde{c}\tilde{c}}\mathbf{Z}_{\tilde{c}\tilde{c}}^{+}\mathbf{Z}_{\tilde{c}\tilde{c}} - \mathbf{Z}_{\tilde{c}\tilde{c}}^{+}\mathbf{Z}_{\tilde{c}\tilde{c}})\mathbf{H}_{\tilde{c}i} - \mathbf{H}_{\bar{c}i}\} \tag{36}$$

and

$$\mathbf{b}_2\mathbf{a}_2^{-1} = \mathbf{H}_{\tilde{c}\tilde{c}}^{-1}(\mathbf{H}_{\tilde{c}\tilde{c}}\mathbf{Z}_{\tilde{c}\tilde{c}} + \mathbf{I})\mathbf{Z}_{\tilde{c}\tilde{c}}^{+}, \quad \mathbf{a}_1\mathbf{b}_1^{-1} = \mathbf{H}_{\bar{c}\tilde{c}}^{-1}(\mathbf{H}_{\bar{c}\tilde{c}}\mathbf{Z}_{\tilde{c}\tilde{c}} + \mathbf{I})\mathbf{Z}_{\tilde{c}\tilde{c}}^{+}. \tag{37}$$

Substituting equations (36) and (37) into equation (35), gives

$$\mathbf{H}_{II} = \mathbf{H}_{ii} + \mathbf{H}_{i\tilde{c}}\mathbf{D}^{+}\mathbf{H}_a + \mathbf{H}_{i\bar{c}}\mathbf{D}^{+\mathrm{T}}\mathbf{H}_b,$$

$$\mathbf{H}_{I\bar{C}} = \mathbf{H}_{i\tilde{c}}\mathbf{D}^{+}\mathbf{H}_c - \mathbf{H}_{i\bar{c}}\mathbf{D}^{+\mathrm{T}}\mathbf{H}_{\bar{c}\bar{c}},$$

$$\mathbf{H}_{I\tilde{C}} = \mathbf{H}_{i\bar{c}}\mathbf{D}^{+\mathrm{T}}\mathbf{H}_d - \mathbf{H}_{i\tilde{c}}\mathbf{D}^{+}\mathbf{H}_{\tilde{c}\tilde{c}},$$

$$\mathbf{H}_{\bar{C}\bar{C}} = \mathbf{H}_{\bar{c}\tilde{c}}\mathbf{D}^{+}\mathbf{H}_c,$$

$$\mathbf{H}_{\bar{C}\tilde{C}} = -\mathbf{H}_{\bar{c}\tilde{c}}\mathbf{D}^{+}\mathbf{H}_{\tilde{c}\tilde{c}}, \quad \mathbf{H}_{\tilde{C}\tilde{C}} = \mathbf{H}_{\tilde{c}\tilde{c}}\mathbf{D}^{+\mathrm{T}}\mathbf{H}_d, \tag{38}$$

where

$$\mathbf{H}_a = (\mathbf{H}_{\tilde{c}\tilde{c}}\mathbf{Z}_{\tilde{c}\bar{c}} - \mathbf{H}_{\tilde{c}\tilde{c}}\mathbf{Z}_{\tilde{c}\tilde{c}}\mathbf{Z}_{\tilde{c}\tilde{c}}^{+}\mathbf{Z}_{\tilde{c}\bar{c}} - \mathbf{Z}_{\tilde{c}\tilde{c}}^{+}\mathbf{Z}_{\tilde{c}\bar{c}})\mathbf{H}_{\bar{c}i} - \mathbf{H}_{\tilde{c}i},$$

$$\mathbf{H}_b = (\mathbf{H}_{\bar{c}\tilde{c}}\mathbf{Z}_{\tilde{c}\tilde{c}} - \mathbf{H}_{\bar{c}\tilde{c}}\mathbf{Z}_{\tilde{c}\tilde{c}}\mathbf{Z}_{\tilde{c}\tilde{c}}^{+}\mathbf{Z}_{\tilde{c}\tilde{c}} - \mathbf{Z}_{\tilde{c}\tilde{c}}^{+}\mathbf{Z}_{\tilde{c}\tilde{c}})\mathbf{H}_{\tilde{c}i} - \mathbf{H}_{\bar{c}i},$$

$$\mathbf{H}_c = (\mathbf{H}_{\tilde{c}\tilde{c}}\mathbf{Z}_{\tilde{c}\tilde{c}} + \mathbf{I})\mathbf{Z}_{\tilde{c}\tilde{c}}^{+}, \quad \mathbf{H}_d = (\mathbf{H}_{\bar{c}\tilde{c}}\mathbf{Z}_{\tilde{c}\tilde{c}} + \mathbf{I})\mathbf{Z}_{\tilde{c}\tilde{c}}^{+}. \tag{39}$$

There is only one inverse operation for the frequency response functions in equation (38), and that is $\mathbf{D}^{+}$. It is the same as the Jetmundsen method as shown in equation (3). Therefore, the computation time and the sensitivity to noise in the FRF data are basically the same for both coupling methods. The computation of $\mathbf{Z}_{\tilde{c}\tilde{c}}^{+}$ should not present a problem since matrix $\mathbf{Z}_{\tilde{c}\tilde{c}}$ is given analytically and its size is relatively small.

The pseudo-inverse, $\mathbf{D}^{+}$, can be calculated using SVD. Performing an SVD on matrix $\mathbf{D}$, which has dimension $(n_{\bar{c}} \times n_{\tilde{c}})$, gives

$$\mathbf{D} = \mathbf{U}\mathbf{S}\mathbf{V}^{h}. \tag{40}$$

If the matrix $\mathbf{D}$ is ill-conditioned or even singular, the singular-value truncation technique will be applied by setting a certain threshold value *tol* and truncating the singular values which are smaller than *tol*. If the remaining number of singular values is r, then

$$\mathbf{D}^{+} = \mathbf{V}_r\mathbf{S}_r\mathbf{U}_r^{h}. \tag{41}$$

The dimensions of $\mathbf{V}_r$, $\mathbf{S}_r$ and $\mathbf{U}_r^{h}$ are $(n_{\tilde{c}} \times r)$, $(r \times r)$ and $(r \times n_{\bar{c}})$ respectively.

4. CASE STUDIES

Two numerical case studies are presented in this section. These examples are designed to emphasize the advantages of the newly developed GJDM for coupling analysis and to demonstrate the use of the new technique in the stage of product design.

The first case study is designed to show how the properties of typical joint parameters, mainly stiffness and damping, affect the coupling results. In the second case study, a larger finite element model is used to investigate the high order mode truncation effect and tolerance to noisy data. The results in both the cases are compared with those obtained from the standard Jetmundsen method.

4.1. CROSS BEAM STRUCTURE

4.1.1. *Description of the structure*

Two identical beams are placed horizontally at right angles and are connected vertically via another very short beam which plays the role of the joint. The boundary condition of the assembled structure is free–free as shown in Figure 1. The lower beam is substructure A and the upper beam is substructure B. The length of each of the substructures is 419 mm and the length of the joint is 3 mm. The cross-section of the substructures is rectangular, 30 mm $\times$ 5 mm. The cross-section of the joint beam is circular with diameter $\phi = 8$ mm.

Each substructure model is divided evenly into 10 Timoshenko beam elements. The joint is described by a single beam element which has six degrees of freedom at each end and whose mass and stiffness matrices are formed by a standard finite element model. Proportional damping is introduced to generate complex frequency response functions for both substructures and to model the joint. The assumed proportional viscous damping model for the joint is described by

$$\boldsymbol{c} = \beta \boldsymbol{k}. \tag{42}$$

If the mass of the joint is neglected, then the describing matrix of the joint becomes

$$\boldsymbol{Z}(\omega) = \boldsymbol{k} + \mathrm{i}\omega\boldsymbol{c} = \boldsymbol{k}(1 + \mathrm{i}\omega\beta). \tag{43}$$

4.1.2. *Coupling analysis by using GJDM*

To validate the GJDM for coupled structure analysis, i.e., its theory and algorithm, the coupling analysis result is compared with that of the complete assembled finite element

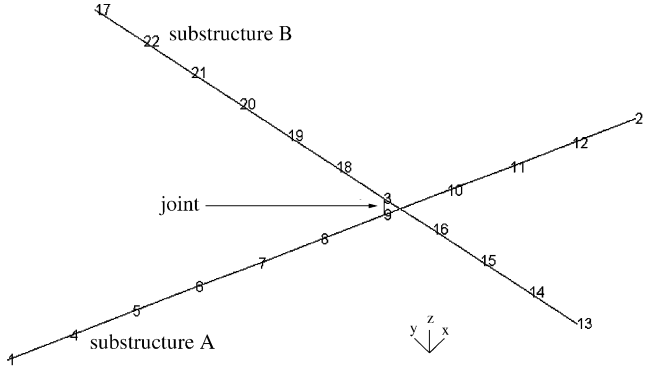

Figure 1. Cross beam structure.

model. In this comparison, the joint parameters prepared for coupling analysis are set to be the same as those used in the assembled finite element model. Based on noise-free input FRFs, all the frequency response functions of the assembled structure are predicted accurately. One of the predicted FRFs is given in Figure 2 overlaid on the corresponding exact result.

One of the advantages of the GJDM is that the joint parameters can be modified independently. This advantage makes it possible for the dynamic characteristics of a structure to be tuned to some extent by varying the joint parameters only. In other words, the joints, which are normally the most difficult parts in finite element modelling, can be completely separated from the substructures and studied independently. After the joint parameters are properly adjusted, they can be used together with frequency response functions of the individual substructures to implement the coupling analysis. In the case shown in Figure 1, for instance, if we increase the damping of the joint by setting a larger β value in equation (42), $\beta = 1 \times 10^{-5}$, the coupling analysis will then perform the effect of this perturbation, as shown in Figure 3 in which the proportional damping factor for the assembled structure is 5×10^{-7}.

The flexibility of changing joint parameters cannot be so easily achieved in the assembled finite element model. This means that the new coupling analysis not only saves computation cost by breaking down a large structure into smaller substructures, but also solves problems which cannot be worked out efficiently using the assembled finite element model.

4.1.3. *Application of Jetmundsen coupling method*

If this same coupling problem is dealt with using the Jetmundsen coupling method, the joint has to be assigned to belong to one of the substructures. This will generally bring the problem that the modification of joint parameters will no longer be achieved so flexibly. Any small change of joint parameters will result in the need for a reanalysis of the substructure to which the joint is attached. This is time consuming if the number of

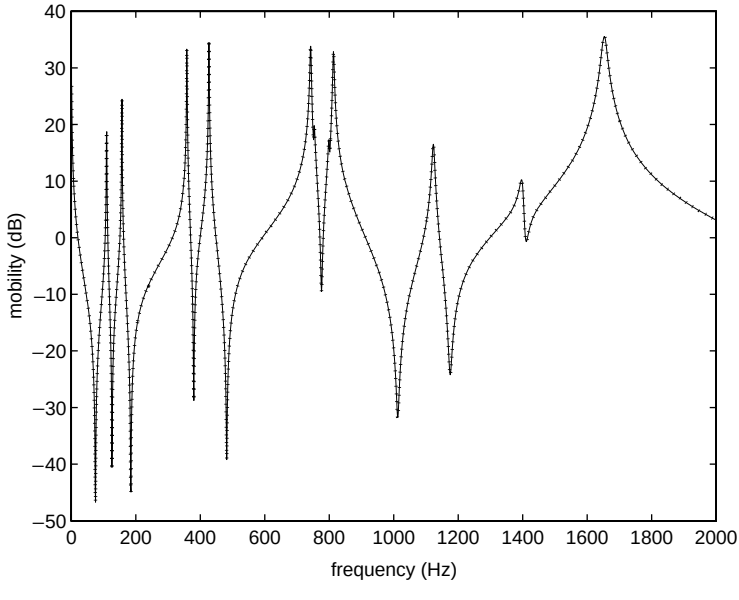

Figure 2. Validation of GJDM:· · · ·, assembled FE; ——, GJDM coupling.

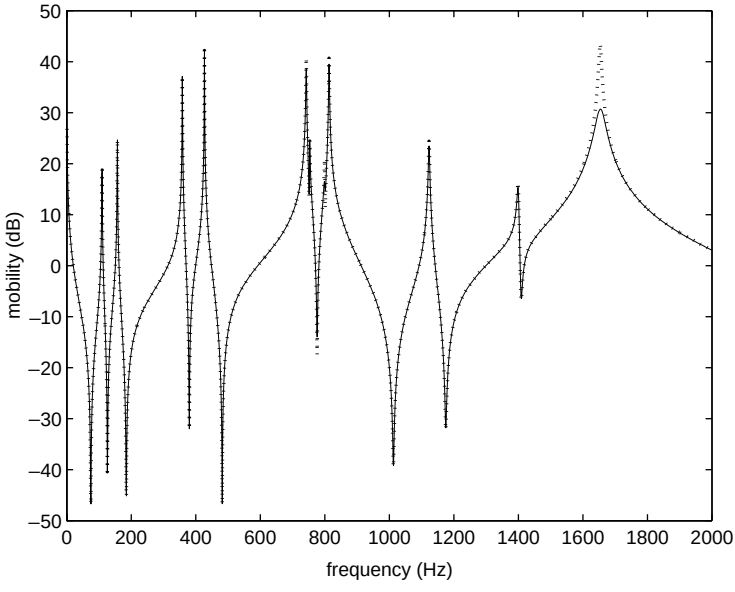

Figure 3. Coupling result of increasing the joint damping: · · · · , assembled FE; ——, GJDM coupling.

degrees of freedom of the substructure is large or if the modification needs to be done a number of times.

In this simple case, the coupling result of the Jetmundsen method can be as accurate as that of the new method, as shown in Figure 2. The tolerance to noisy input data is also more or less the same, according to the analysis in section 3. More detail comparisons between these two FRF coupling methods will be given and discussed next for a more complicated case study, a plate coupled with a beam.

4.2. PLATE COUPLED TO BEAM

4.2.1. *Description of the structure*

The second case study is based on a brass plate shown in Figure 4 and a brass beam shown in Figure 5 which are coupled together using a steel bolt. The alignment of the coupled system is shown in Figure 6. The detail of the connection joint is shown in Figure 7 where the size of the steel bolt is M4. The material properties of the structure are listed in Table 1.

4.2.2. *Coupling analysis* 1*: Jetmundsen method*

The plate is taken as substructure A and the beam together with the bolt are taken as substructure B. The FRFs of the two substructures, A and B, are generated from the modal analysis of their finite element models. The 4-node 20-d.o.f. plate elements are used to model the plate, and Timoshenko beam elements are used to analyze the beam, substructure B (see Figure 8). FRFs were generated using the mode superposition method: the numbers of modes used were:

$$m_A = 300 \ (90 \text{ kHz}) \quad \text{and} \quad m_B = 50 \ (20 \text{ kHz}).$$

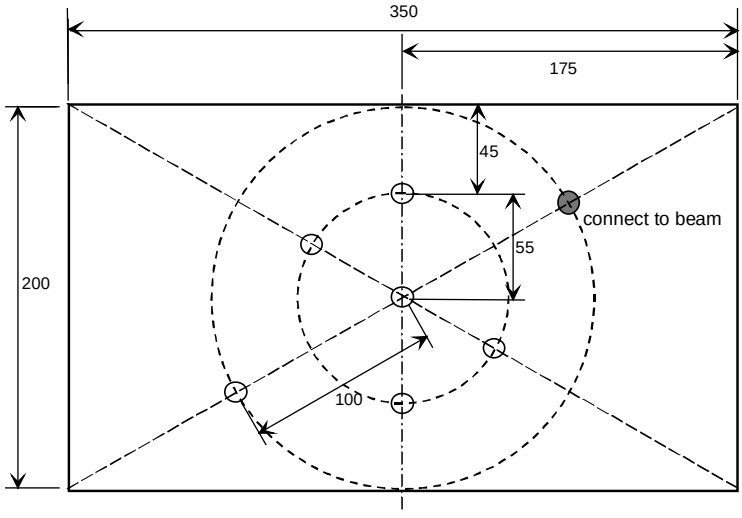

Figure 4. Brass plate, thickness 3 mm.

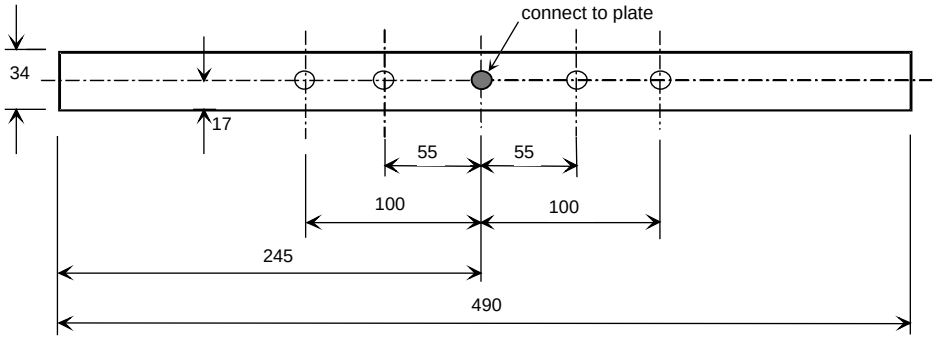

Figure 5. Brass beam, thickness 3 mm.

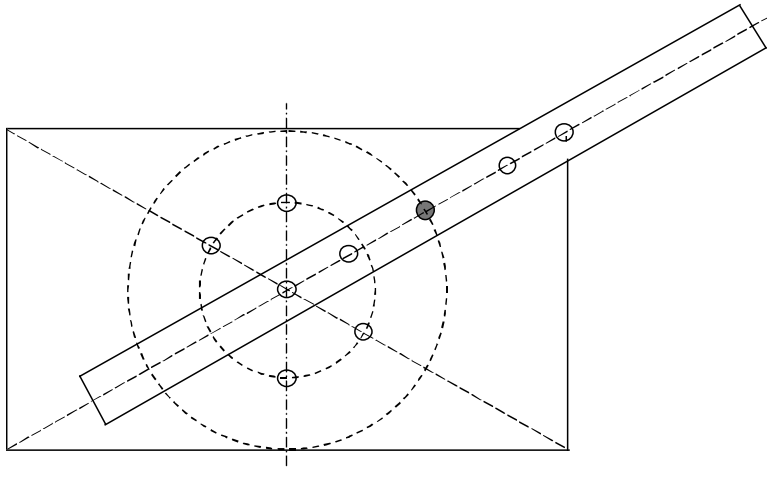

Figure 6. The assembled structure.

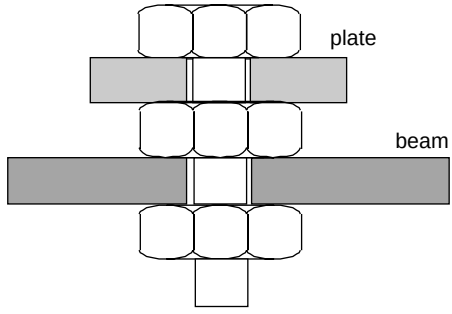

Figure 7. Bolt connection.

TABLE 1

Material properties

Material	Young's modulus	The Poisson ratio	Density
Brass	$1{\cdot}10 \times 10^{11}$ N/m^2	0·29	$8{\cdot}54 \times 10^3$ kg/m^3
Steel	$2{\cdot}10 \times 10^{11}$ N/m^2	0·30	$7{\cdot}80 \times 10^3$ kg/m^3

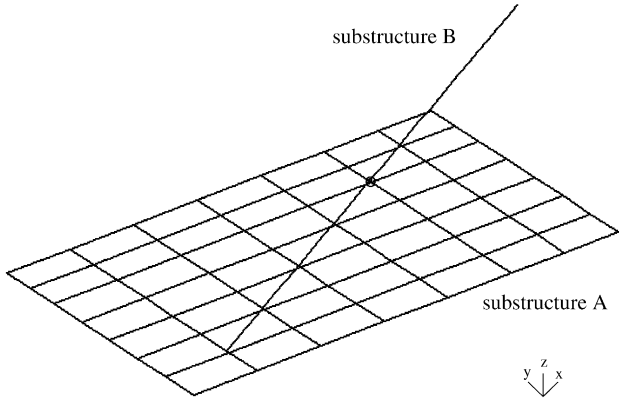

Figure 8. FE mesh for coupling analysis.

FRFs of the coupled structure were obtained by implementing the analysis based on the Jetmundsen method. Input data were the FRFs of the substructures. The result is compared with the "exact" FRFs which were produced by analyzing the finite element model of the whole assembled structure. One FRF from the coupling analysis results, the point FRF H_{5z5z}, i.e., the translation point FRF in the z direction of node 5, which is the coupling node on the plate, is shown in Figure 9 overlaid with its corresponding "exact" FRF. It is seen that the Jetmundsen method works well in general, except for the frequency shift in the frequency range of 800–1200 Hz.

4.2.3. *Coupling analysis 2: general joint description method*

In this analysis, the plate is still taken as substructure A but the beam alone is taken as substructure B, excluding the bolted joint. FRFs of the two substructures, A and B, are

also generated from the modal analyses of their finite element models using mode superposition method.

The bolt which connects plate and beam is defined by a beam element. Since the mass of the bolt is very small compared with either of the substructures (the plate or the beam), only the bolt stiffness is taken into account to construct the joint description impedance matrix, $\boldsymbol{Z}$. The compatibility of degrees of freedom is considered in forming the matrix, $\boldsymbol{Z}$. The beam element has six d.o.f.s at the boundary connecting it to the beam ($n_{\tilde{c}} = 6$) and five d.o.f.s at the boundary connecting it to the plate ($n_{\bar{c}} = 5$). Therefore, the dimension of matrix $\boldsymbol{Z}$ is (11×11).

FRFs of the coupled structure were obtained by implementing the programme of the general joint description method. Input data were the FRFs of the substructures as well as the joint description matrix, $\boldsymbol{Z}$. The result was validated by the "exact" FRFs which were produced by analyzing the finite element model of the whole assembled structure. One FRF of the coupled structure analysis results, the point FRF, H_{5z5z}, which is the coupling node on the plate, is shown in Figure 10 overlaid with its corresponding "exact" FRF. It is clear from Figure 10 that the coupling analysis yields a very good result. There are no significant frequency shifts as shown in Figure 9.

4.2.4. *Substructure residual effect*

It should be pointed out that there is no substructure residual effect to the coupling analysis result if measured FRFs are used. However, in a numerical study as that presented in this section, it is an important issue for discussion. The numbers of modes used for substructures A and B were 320 and 186, respectively, while the coupling result shown in Figure 10 was achieved by using only the first 300 modes from substructure A and the first 50 modes from substructure B.

To investigate the substructure residual effect, the number of modes used in generating the FRFs was varied. Table 2 shows the numbers of modes of substructure A (plate) which

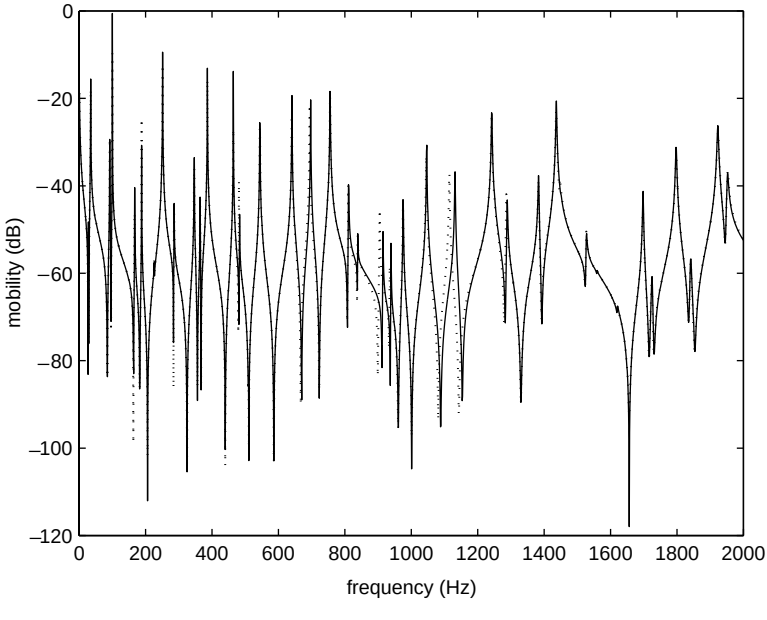

Figure 9. Point FRF H_{5z5z} obtained from the Jetmundsen coupling analysis. —— Jetmundsen method; · · · · , assembled FE.

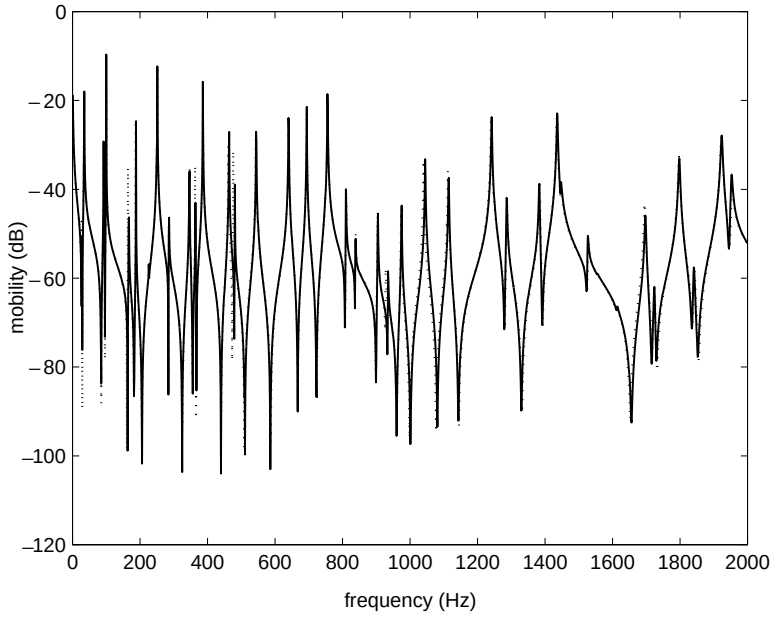

Figure 10. Point FRF H_{5z5z} obtained from the GJDM coupling analysis: · · · · , assembled FE; ——, GJDM method.

TABLE 2

Numbers of modes of substructure A and the highest natural frequencies involved

	$m_A = 130$	$m_A = 150$	$m_A = 200$	$m_A = 250$	$m_A = 300$
f_{m_A} (Hz)	12 875	16 545	28 872	52 693	95 703

were used in this part of the study, together with the corresponding highest natural frequencies. In all cases, the FRFs of substructure B (the beam) were generated using 30 modes, which meant that the highest natural frequency was 7049 Hz.

The coupling analysis results obtained by using different numbers of high order mode truncations are shown in Figure 11. This is the same FRF as that shown in Figure 10, the point FRF, H_{5z5z}. According to the modal analysis of the assembled system finite element model, there are 43 elastic modes in the displayed frequency range of 0–2000 Hz, but not all of them are seen in this point FRF plot. It can be noticed in Figure 11 that only three modes, numbered as 23, 24 and 28, which have the frequency values of 903·7, 927·8 and 1112·3 Hz, respectively, are significantly affected by the high order mode truncations. The rest of the modes are almost consistent with respect to different numbers of mode truncation.

It is found that mode 28 in Figure 11 (the one whose natural frequency is at 1112·3 Hz) is dominated by residuals. Its frequency shifts to a higher value and its amplitude becomes smaller with regard to the decrease of m_A, the number of modes included for generating FRFs of substructure A, the plate. Further calculations show that if m_A is chosen such that $m_A < 120$, this mode will disappear from this FRF plot.

This study shows that the number of modes included in generating the FRFs for substructure A plays a very important role in the accuracy of the coupling result.

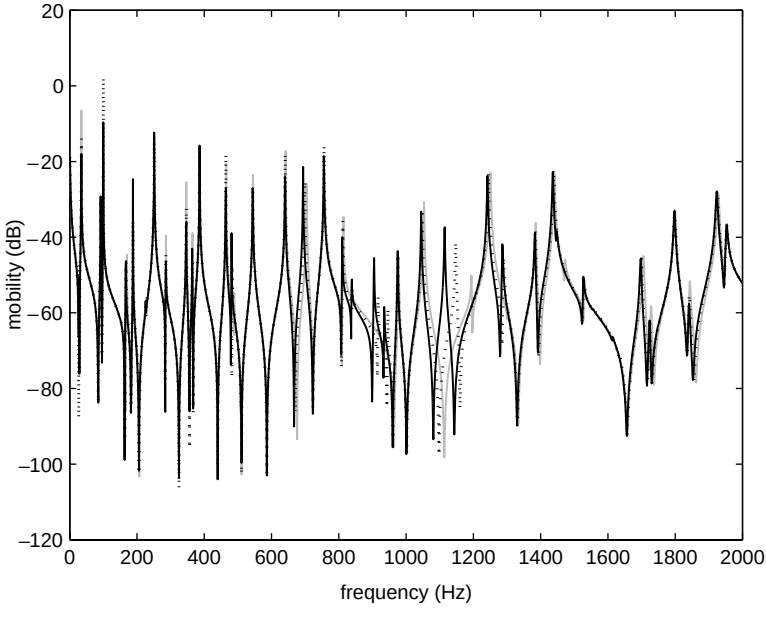

Figure 11. Investigation of residual effect ($m_B = 30$): ——, $m_A = 120$; $\cdots$, $m_A = 200$; ——, $m_A = 300$.

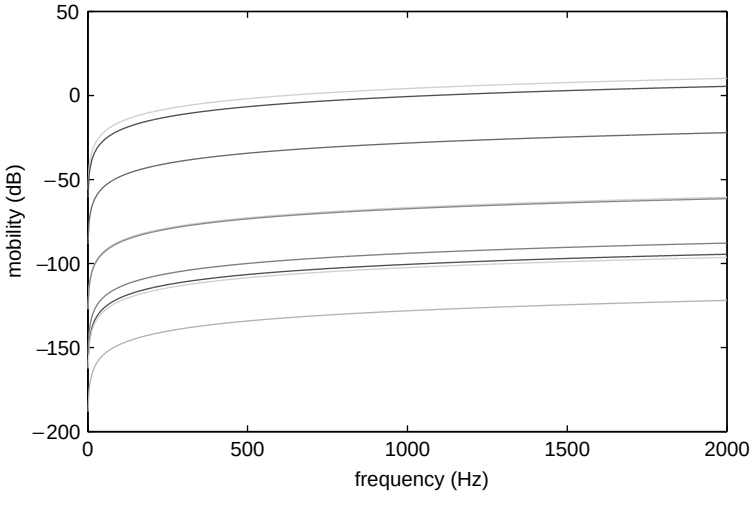

Figure 12. Residual FRFs of substructure A.

The residual FRFs in the frequency range 0–2000 Hz were then generated including the truncated modes, from mode 131 to 300, and are shown in Figure 12. These FRFs are, from top to bottom: $H_{5\theta_x 5\theta_x}$, $H_{5\theta_y 5\theta_y}$, $H_{5\theta_x 5\theta_y}$, $H_{5z5\theta_x}$, $H_{5z5\theta_y}$, H_{5z5z}, H_{5x5x}, H_{5y5y} and H_{5x5y}.

Comparing the amplitudes of these residual FRFs with those of the FRFs used for coupling analysis, which are shown in Figure 13, one can see that these residual FRFs are not negligible even though the truncation frequency is already 6 times of the highest frequency of interest (2000 Hz).

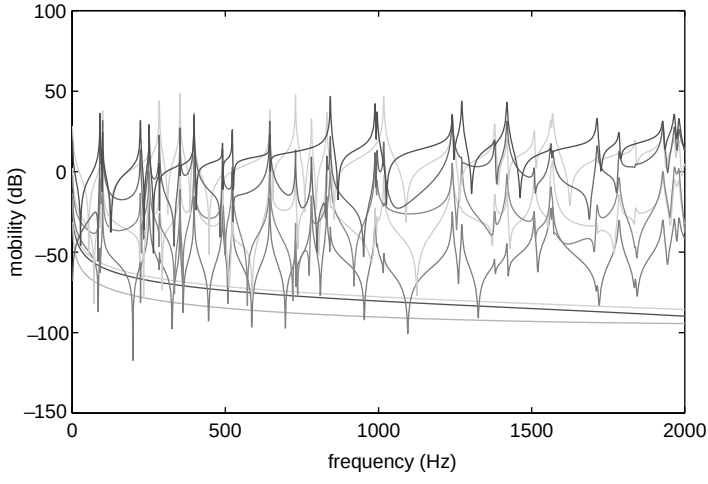

Figure 13. FRFs of plate at coupling d.o.f.s.

Therefore, in principle, the GJDM method is recommended when measured FRFs are available because they do not have mode truncation error. For analytical coupling analysis, the improved CMS method, component mode synthesis with joint involved (CMSJ) [10], should be the first choice. In the cases where FRF coupling method has to be applied, a large number of modes need to be calculated in order to generate the substructures' FRFs.

4.2.5. *Tolerance to noisy data*

The motivation to develop the Jetmundsen method and the GJDM is to permit direct use of measured frequency response functions. Therefore, it is important to verify that these methods can work properly when they are supplied with noise-contaminated data.

If 10% random noise is added to the FRF matrices for both substructures A and B, the coupled structure result obtained from the GJDM previously shown in Figure 10 is shown here in Figure 14.

Following the same procedure, Figure 15 shows the coupling result when the FRF matrices of the substructures are contaminated by 20% random noise.

By applying singular-value truncation to the 20% noise case, in which the threshold was set as $\varepsilon = 10^{-6}$, the result shown in Figure 15 can be improved. To justify the quality of the predicted FRFs which are obtained using noisy FRFs for the substructures, the correlation between the predicted FRF matrices and the exact FRF matrix (FRAC, defined in reference [11]) is calculated. The FRAC values shown in Figure 16 are the correlations of the upper triangle FRF matrices, in which there are 15 FRFs. The corresponding full FRF matrix is shown in equation (44).

$$\mathbf{H}_{\bar{C}} = \begin{bmatrix} H_{5x5x} & H_{5x5y} & H_{5x5z} & H_{5x5\theta_x} & H_{5x5\theta_y} \\ H_{5y5x} & H_{5y5y} & H_{5y5z} & H_{5y5\theta_x} & H_{5y5\theta_y} \\ H_{5z5x} & H_{5z5y} & H_{5z5z} & H_{5z5\theta_x} & H_{5z5\theta_y} \\ H_{5\theta_x5x} & H_{5\theta_x5y} & H_{5\theta_x5z} & H_{5\theta_x5\theta_x} & H_{5\theta_x5\theta_y} \\ H_{5\theta_y5x} & H_{5\theta_y5y} & H_{5\theta_y5z} & H_{5\theta_y5\theta_x} & H_{5\theta_y5\theta_y} \end{bmatrix}. \tag{44}$$

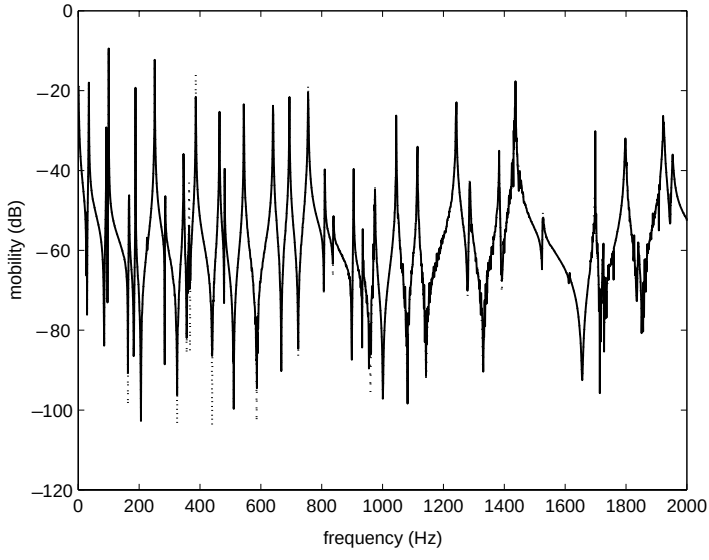

Figure 14. Coupling result (GJDM) when 10% noise in input FRFs:· · · ·, exact; ——, 10% noise.

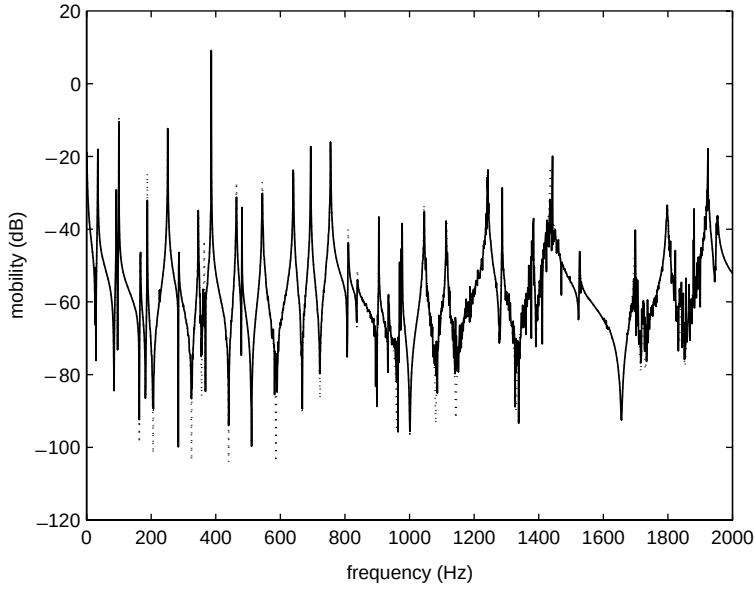

Figure 15. Coupling result (GJDM) when 20% noise in input FRFs:· · · ·, exact; ——, 20% noise.

It is shown that GJDM is generally not sensitive to noise. All point FRFs are very well predicted, even in the 20% noise case. The results which have low FRAC values are basically those FRFs which have low response levels. The FRAC values increase significantly when singular-value truncation is applied to the 20% noise case. They are almost the same as the 10% noise case without the singular-value truncation.

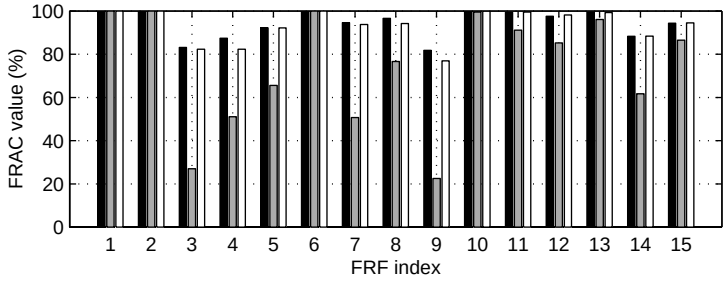

Figure 16. FRACs: ▬ 10% noise; ▬, 20% noise; ▭ 20% with σ-value truncation.

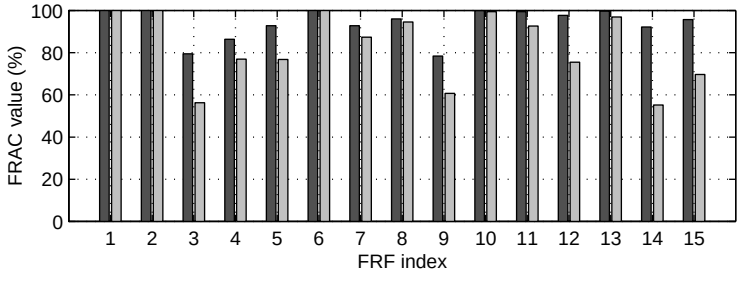

Figure 17. FRAC of the two coupling methods: ▬, GJDM; ▬, K-J method.

4.2.6. *Comparison between Jetmundsen method and GJDM*

The coupled structure analysis results produced by the Jetmundsen method and the GJDM are compared under the same conditions: the same numbers of modes are used to generate the FRFs of the substructures and these FRFs are free of noise. The FRAC—correlation between the coupling analysis results and the assembled finite element analysis result—is calculated and displayed in Figure 17.

It is seen that the GJDM is universally superior to the Jetmundsen method in this example.

5. CONCLUSIONS

The development of a new FRF coupling analysis method, the generalized joint describing method (GJDM), has been reported and shown to have the following advantages compared with the conventional Jetmundsen method:

- The joint is completely separated from the main substructures, and joint parameters are modified independently. The substructures do not need to be reanalyzed with respect to the variation of joint parameters.
- The number of coupling degrees of freedom in one substructure can be different to that for another substructure to accommodate non-conforming interfaces [12].
- The joint describing impedance matrix is made independent from the substructures. Its stiffness and damping can be adjusted to fulfil the requirement of the system response. This is not only an advantage for substructure coupling analysis but also provide a technique for damper design in vibration control.

REFERENCES

1. R. R. Craig Jr 2000 *Proceedings of* 18*th IMAC*, *San Antonio*, *TX*, 899–908. A brief tutorial on substructure analysis and testing.
2. D. J. Ewins 2000 *Modal Testing*: *Theory*, *Practice and Application*. Philadelphia, PA: Research Studies Press Ltd; 2nd edition.
3. A. P. V. Urgueira 1989 *Ph.D. Thesis*, *Department of Mechanical Engineering, Imperial College*, Dynamic analysis of coupled structures using experimental data.
4. B. Jetmundsen, R. L. Bielawa and W. G. Flannelly 1988 *Journal of the American Helicopter Society* **33**, 55–64, Generalized frequency domain substructure synthesis.
5. D. Otte, J. Leuridan, H. Grangier and R. Aquilina 1991 *Proceedings of* 9*th IMAC*, *Florence*, *Italy*, 909–918. Prediction of the dynamics of structural assemblies using measured FRF data: some improved data enhancement techniques.
6. L. E. Suarez and E. E. Matheu 1992 *Journal of Vibration and Acoustics* **114**, 209–216. A modal synthesis technique based on the force derivative method.
7. R. E. D. Bishop and D. C. Johnson 1960 *The Mechanics of Vibration*. Cambridge: Cambridge University Press.
8. J. V. Ferreira and D. J. Ewins 1996 *Proceedings of* 14*th IMAC*, *Dearborn*, *MI*, 1034–1040. Nonlinear receptance coupling approach based on describing functions.
9. Y. Ren and C. F. Beards 1995 *Journal of Sound and Vibration* **185**, 845–866. On substructure synthesis with FRF data.
10. W. Liu 2000 *Ph.D. Thesis*, *Department of Engineering*, *Imperial College*. Structural dynamic analysis and testing of coupled structures.
11. W. Heylen and P. Avitabile 1998 *Proceedings of* 16*th IMAC*, *Santa Barbara*, *CA*, 207–214. Correlation considerations—Part 5 (degree of freedom correlation techniques).
12. C. Farhat and M. Geradin 1992 33*rd SDM Conference*, *Dallas*, *TX*, AIAA paper 92-2383-CP, 1783–1796. A hybrid formulation of a component mode synthesis method.

APPENDIX A: NOMENCLATURE

A, B	subscripts denoting substructures A and B
i, c	subscripts denoting internal and coupling co-ordinates in substructures
$\bar{c}, \tilde{c}$	subscripts denoting coupling co-ordinates in substructures A and B
$\bar{C}, \tilde{C}$	subscripts denoting coupling co-ordinates of substructures A and B in the assembly
I	subscripts denoting internal co-ordinates in assembly
$\mathbf{H}$	frequency response function
$\mathbf{F}$	force applied onto the assembly
$\mathbf{x}$	displacement vector of substructures
$\mathbf{X}$	displacement vector of the assembly
$\boldsymbol{f}$	force applied onto the joint
$\boldsymbol{x}$	displacement vector the joint
$\boldsymbol{Z}$	impedance matrix of joint